Letter | Editors' Suggestion

Charge separation and directed migration of photoelectrons in $LiNbO_3$: Fe crystals after excitation by nanosecond laser pulses

F. S. Pilyak,[1,2] E. I. Mareev,[1,*] A. G. Kulikov,[1,2,†] N. M. Asharchuk,[1] N. N. Obydennov,[1,3] Y. V. Pisarevsky,[1,2] A. E. Blagov,[1] F. V. Potemkin,[3,‡] and M. V. Kovalchuk[1]

[1]*Kurchatov Complex for Crystallography and Photonics of NRC "Kurchatov institute", Leninskiy pr-kt 59, Moscow, Russia*

[2]*Kurchatov Complex for Synchrotron and Neutron Investigations of NRC "Kurchatov institute", Pl. akademika Kurchatova 1, Moscow, Russia*

[3]*Faculty of Physics, M. V. Lomonosov Moscow State University, Leninskie Gory bld. 1/2, 119991 Moscow, Russia*

(Received 11 March 2024; revised 7 June 2024; accepted 22 July 2024; published 9 September 2024)

Unusual time-delayed changes in the x-ray diffraction parameters of $LiNbO_3$ and $LiNbO_3$: Fe crystals were observed under nanosecond laser impact. Subnanosecond time resolution in the registration of diffraction rocking curve (DRC) dynamics was achieved through the synchronization of a 4 ns laser pulse with the circulation phase of electron bunches within a synchrotron storage ring. The response of the crystals to optical impact resulted in a reversible center-of-mass shift and integral intensity decrease of the DRC recovering in ∼35 ns. The dynamics of lattice deformation indicates the process of formation and subsequent decay of an electrical charged layer near the surface due to directed migration of photoelectrons as a result of the bulk photovoltaic effect. The drop in the integral intensity of the DRCs is apparently caused by a running wave generated by a sharp change in the deformation of the crystal lattice. In the case of the nominally undoped crystal, the time-delayed processes occur within the same time interval but with significantly smaller amplitudes.

DOI: 10.1103/PhysRevB.110.L100302

Introduction. Generation of adjustable strains is a promising approach to controlling the physical properties of functional crystalline materials, which opens opportunities for creating the next generation of energy-efficient sensors, computing devices, and information storage systems [1–4]. The formation of strains with high spatial localization in crystal near-surface layers can be achieved through external influences of various natures [5,6]. One of the possible methods for efficient, fast, and contactless control of deformations is based on the combination of the bulk photovoltaic effect (BPE) [7] and the converse piezoelectric effect—the piezophotovoltaic effect [8]. According to the BPE mechanism, the excited electrons migrate in a specific direction with relevance to the photovoltaic tensor [9–11]. Moreover, drift and diffusion can also contribute to the movement of the charge carriers [12]; for example, in narrow-band-gap semiconductors, the Dember effect would play the dominant role [13]. However, the BPE even occurs at impurities of low-absorbing dielectrics, which makes it the most controllable for memory devices [14]. The parameters of the BPE-induced electric field (localization area, electric field intensity, and formation time) can be controlled via changes of the laser impact parameters. This provides an opportunity to generate specific strains in the crystal. Special attention should be given to the temporal characteristics of the charge separation process that leads to the formation of an electric field within the mechanism of the BPE. This process was mainly investigated using electrophysical methods [15–17], particularly by the Hall method which, however, allows data to be recorded only integrally [18]. Recently, notable advancements have been made in time-resolved x-ray optical experimental techniques, which have been used to explore laser-induced physical processes and phenomena encompassing phase transitions, shock-wave generation, phonon dynamics, and crystal lattice deformation [19,20]. The potential to retrieve the dynamics of these processes has been facilitated by the evolution of x-ray free-electron lasers [21] and attosecond laser systems [22], alongside the progress in synchrotron radiation sources and laser-plasma x-ray sources [23,24]. The latter has made it possible to measure x-ray diffraction in a pump-probe regime to reveal polarized-dependent photocurrent in lithium niobate with a picosecond resolution [25]. For diagnostics of processes induced by short (nanosecond) laser pulses, thoughtful consideration is essential when selecting an x-ray radiation source and experimental technique. The use of high-intensity x-ray sources brings about associated challenges due to the substantial power applied on the object, which can lead to its destruction or the initiation of various nonlinear processes, frequently complicating the clear interpretation of experimental results. Synchrotron radiation sources stand out as some of the most practical x-ray radiation sources for investigating phenomena occurring on the time scale from hundreds of picoseconds up to milliseconds. Leveraging laser-synchrotron complexes [26] enables precise time-resolved measurements with subnanosecond resolution and the acquisition of high-quality statistical data. In this letter, the approach outlined in Ref. [26] was optimized to perform time-resolved x-ray diffraction analyses of the deformation dynamics of nominally pure $LiNbO_3$ and $LiNbO_3$: Fe at a synchrotron radiation (SR)

*Contact author: mareev.evgeniy@physics.msu.ru
†Contact author: ontonic@gmail.com
‡Contact author: potemkin@physics.msu.ru

 ©2024 American Physical Society

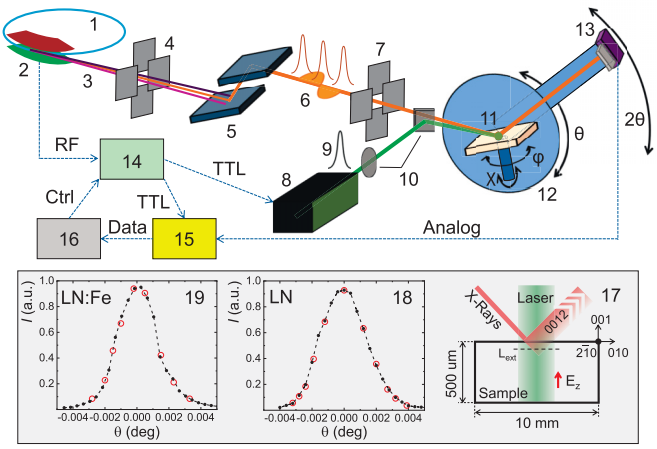

FIG. 1. Schematic diagram of the x-ray diffraction experiment: (1) The synchrotron radiation (SR) source; (2) bending magnet; (3) white incident SR beam; (4) input mask of the white beam; (5) monochromator with a pair of Si 111 crystals; (6) monochromatic σ-polarized x-ray beam with a bunch time structure of the storage ring; (7) x-ray slits; (8) laser; (9) pulsed laser radiation; (10) optical elements; (11) sample; (12) multicircle goniometer with θ, 2θ, ϕ, and χ axis; (13) avalanche photodiode detector; (14) FPGA-based TTL synchronization system with a delay control (Ctrl) relative to radiofrequency (RF) signal on the input; (15) high-speed oscilloscope; (16) computer; (17) scheme of the sample illumination by laser and x-ray radiation; extinction length of x rays $L_{ext} = 3.7\,\mu$m corresponds to the 0012 reflection; E_z is a component of photoinduced electric field; and (18) and (19) rocking curves of LN and LN : Fe, respectively (reflection 0012), obtained by mechanical step-mode θ scan (black dashed line) and angular positions for the time-resolved measurements (red open circles).

source under nanosecond laser impact. By synchronizing the laser and detection system with the circulation period of the electron bunches in the storage ring, a time resolution <1 ns was achieved.

Experiment and methodology. We performed a comparative analysis of lattice dynamics induced by laser impact onto two specimens: nominally pure lithium niobate $LiNbO_3$ (LN) and iron-doped LN : Fe (Fe_2O_3 0.1 wt. %). The samples for analysis were fabricated from monodomain single crystals in the form of plane-parallel rectangular polished plates with (001) orientation, cross-sectional dimensions of 10×10 mm, and a thickness of 0.5 mm. The experimental setup for time-resolved x-ray diffractometry was assembled at the RKFM beamline of the synchrotron radiation source KISI-Kurchatov, National Research Center "Kurchatov Institute," the experimental setup is shown in Fig. 1. In the experiments, a 12 keV x-ray beam (0.5×0.2 mm) after monochromator was directed onto the sample, mounted in an optically transparent crystal holder on the diffractometer. The sample was aligned to the 0012 reflection with a Bragg angle of $\theta = 26.562^\circ$ and an extinction length of $L_{ext} = 3.7\,\mu$m. The intensity of the beam, detected by an avalanche photodiode detector was collected through the digital oscilloscope. An optical impact was performed by a pulsed laser system with a duration of $\sim$4 ns, a wavelength $\lambda_{2\omega} = 532$ nm, and energy up to $\sim$20 mJ in each pulse. A system of mirrors directed the laser radiation onto a long-focus lens ($\sim$250 mm), ensuring the overlap of the optical and x-ray beams in the region on the sample surface (diameter of the laser spot projection is $\approx$2.0 mm). The laser beam was normally incident on the sample with linear polarization directed along the crystallographic x axis [$2\bar{1}0$]. The impact of the laser pulses on the sample was synchronized with the circulation phase of electron bunches in the synchrotron storage ring [27]. The technique of time-resolved x-ray diffractometry involves recording the time evolution of diffracted x-ray radiation intensity at various angular positions of the diffraction rocking curve (DRC) [28,29]. All details about experimental technique and methodology are described in the Supplemental Material [30]. The feature of our experiments is the use of laser pulses of relatively low intensity. As a result, we disregard potential nonlinear optical effects, particularly the excitation of two-photon processes, as their contribution is four times lower, considering two-photon absorption coefficient for 532 nm wavelength $\beta = 1.210^{-3}$ m/GW [31]. Therefore, we consider that the green laser activates the generation of photoelectrons only from in-gap states which correspond to impurities in the crystal.

Experimental results. The dynamics of DRC of the 0012 reflection was recorded for LN : Fe and LN crystals. Figure 2(a) demonstrates a segment of the three-dimensional map with a duration of 900 ns for the LN : Fe crystal, which encompasses the interval of laser pulse impact (4 ns) and two full circulation periods of the electron bunches in the storage ring of $T_{sr} = 414$ ns each. Figures 2(b) and 2(c) illustrate segments for the doped and nominally pure samples, respectively, within a range of -50 to $+100$ ns relative to the laser pulse. Figure 3 illustrates alterations in DRC parameters occurring within the 0–35 ns range following the laser pulse impact, notably demonstrated by a reduction in integral intensity. This observation is prominently evident when reviewing the DRC profiles obtained at various points along the time coordinate. In Fig. 3(a), a series of DRCs for the LN : Fe crystal is presented, corresponding to the specific changes in the DRC dynamics from Fig. 2(b). A dashed line indicates the initial DRC of the experimental sample. It is evident from the figure that the laser pulse impact leads to a significant decrease in the peak intensity, accompanied by a complex alteration in the shape of the peak. These morphological alterations also induce a shift in the center of mass of the curve. The DRC parameters are observed to return to their initial state at $\sim$35 ns after laser pulse impact. Figure 3(b) shows the time evolution of both the DRC center of mass position and its integral intensity for the LN : Fe and nominally pure LN crystals. Analysis of Figs. 2 and 3 reveals that the response of experimental samples to the laser impact increase and decays within $\sim$35 ns after laser pulse; thus, DRC parameters have time to return to their original values before the next pulse. In the interval of 0–20 ns after laser impact, a decrease in the integral intensity of the diffracted x-ray beam is observed (by $\sim$60%), and the position of the DRC peak shifts toward smaller angles, reaching a value of -0.7 arcsec relative to the initial averaged value after 14 ns. This is followed by a symmetrical shift of the DRC toward greater angles, reaching $+0.7$ arcsec, with the subsequent relaxation of the parameters to its initial values. On the submillisecond to millisecond time

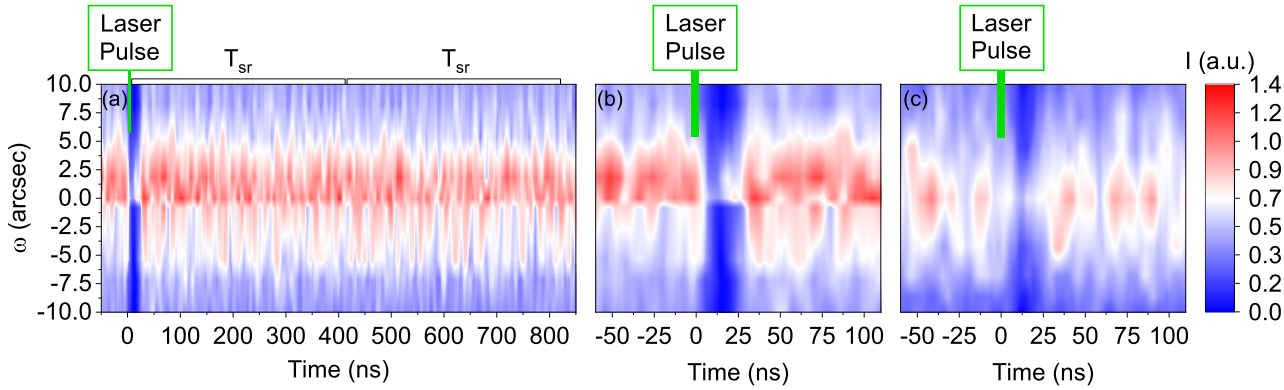

FIG. 2. (a) Dynamics of diffraction rocking curve (DRC) of a LN : Fe crystal exposed to a 4 ns laser pulse with ∼1 J/cm^2 fluence over a time range of 900 ns, obtained for the 0012 reflection. T_{sr} is the storage ring period of the KISI-Kurchatov synchrotron. The DRC dynamics under the impact of a laser pulse on enlarged scale for (b) an iron-doped LN : Fe and for (c) an undoped LN samples.

scale [32], we did not observe thermal drift of the DRC or changes in its shape. Furthermore, over several hours of continuous operation, no shifts in the DRC were detected. Based on these data, it seems reasonable to suggest that temperature effects do not influence the experiments. The obtained results could be applied for the characterization of the recorded process. The shift of the DRC peak allows us to quantify the electric field strength of the BPE and the magnitude of deformations. Furthermore, the temporal characteristics of the process offer insights into the mechanism of its occurrence. Both the doped and nominally pure samples exhibit responses to the laser pulse within an identical time window. However, the doped sample demonstrates a noticeably more pronounced change in the integral intensity of the DRC.

Discussion. An intriguing aspect of the observed effect is the delay in the response of the DRC after the nanoseond laser pulse impact, occurring on the nanosecond time scale. This time scale is considerably longer than the time delays associated with the formation and propagation of possible light-induced strain waves, which are usually bipolar [33] and previously were observed for $BiFeO_3$ [34], GaAs [35], and PTO [36]. In our case, considering the sound velocity (v_L = 7.33 nm/ns for longitudinal and v_T = 3.57 nm/ns for shear wave types) [37], the propagation of such a wave through the extinction depth should occur within hundreds of picoseconds, and its observation on the nanosecond time scale is unlikely. Therefore, we could attribute the observed delayed effect to thermalized electrons creating a screening layer near the surface. The internal built-in electric field $E_{\text{int}} \approx$ 2.3–3.5 kV/mm [38,39] caused by the relatively high spontaneous polarization ∼71 μC/cm^2 [40] may be partially screened even before the appearance of photoelectrons, for example, by vacancies or electrons from impurities. However, due to the low dark conductivity, the near-surface fields will be weakly expressed. Upon optical photon absorption, the excitation of electrons to the conduction band, i.e., photoelectron generation, occurs from the Fe^{2+} energy level for a doped crystal and from uncontrolled impurities for an undoped one. For lithium niobate with an iron doping of 0.1 wt. % of Fe_2O_3, the concentration of injection centers (Fe^{2+}) was ∼10^{25} m^{-3} [41], and photoelectrons were generated almost uniformly throughout the thickness of the crystal since the measured optical penetration depth of laser radiation in doped lithium niobate is $1/\alpha$ = 0.91 mm. Nonthermalized laser-induced electrons cause a coherent shift current directed along the spontaneous polarization [42,43]. This shift current makes the greatest contribution

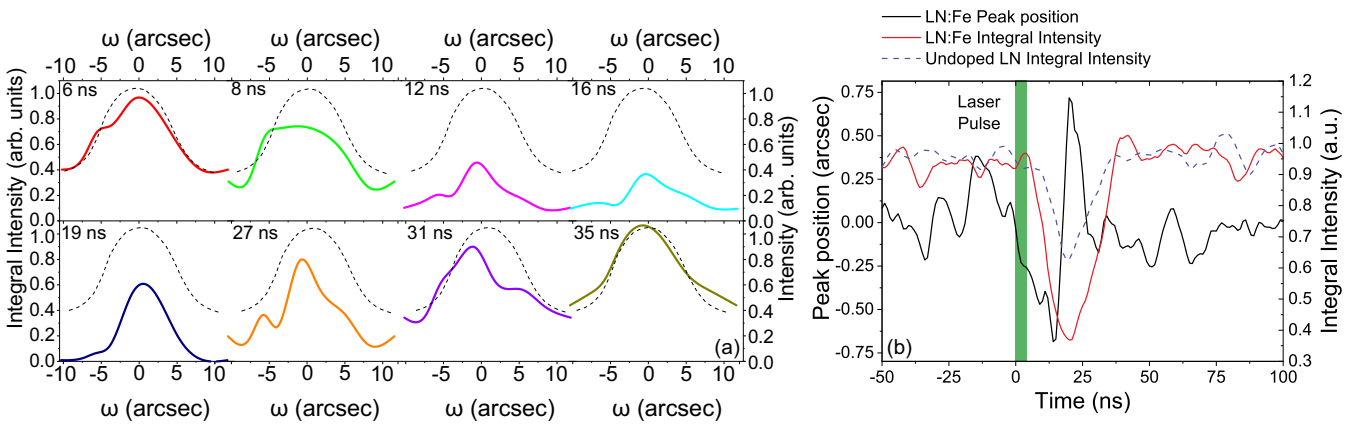

FIG. 3. (a) LN : Fe diffraction rocking curves (DRCs) of 0012 reflection at several time positions after the laser pulse (dotted curve is the initial DRC); (b) the dynamics of the DRC peak position (black line) and the integral intensity (red line) for LN : Fe as well as the dynamics of the integral intensity for undoped LN (blue dashed line) in comparison. Green bar indicates the duration of the optical pulse.

to the formation of BPE in LN under laser impact due to their high mobility 10^{-3} to 10^{-1} m^2 V^{-1} s^{-1}, and in an open-circuit regime, the saturation BPE field values can reach up to 10 kV/mm [12,15]. After transition to the conduction band, laser-induced electrons are thermalized, forming small polarons, and rapidly lose their mobility [44]. Small polarons are trapped in shallow traps associated with Nb^{4+} due to their relatively low mobility of $\mu_p = 10^{-8}$ m^2 V^{-1} s^{-1} [45] and have a relatively longer lifetime up to 10^1 ns and longer [46,47]. The directed migration of polarons leads to the spatial separation of negative and positive electric charges (polarons and holes). Polaron drift current is directed along the polarization and leads to the formation of a screening layer near the surface with fields up to several kV/mm, creating strong piezoelectric deformations in the near-surface region, which distort and split the Bragg peak ~10 ns after laser impact [see Fig. 3(a)]. The piezoelectric deformation of the LN : Fe crystal, retrieved from the shift of the DRC peak, starts with the laser impact and increases to a magnitude of $\Delta d/d = 0.68 \times 10^{-5}$ within 7 ns, corresponding to the screening electric field of $E_{sc} = 1.1$ kV/mm. The variation in polarization charge density on the surface can be estimated as $\delta\sigma_p = jt = Nq\mu_p E_{\text{int}} t$ amounting to ~30 nC/cm^2. The induced screening electric field, with a depth-dependent strength gradient induces a lattice deformation and a shift of the DRC center of mass through the activation of the d_{33} piezoelectric tensor component. This leads to a region of tension (screening near-surface fields) and a region of compression (compensated internal field) within the initial lattice, resulting in asymmetric DRC shape and the formation of peak satellites ~15 ns [see Fig. 3(a)]. Subsequently, after 20 ns, considering the recombination of polarons, the screening field diminishes gradually, and by ~35 ns after the laser impact, the diffraction peak returns to its original symmetric shape. The decrease in DRC integral intensity [Fig. 3(b)] within the same time frame may be linked to the propagation of a running strain wave. The intricate dynamics of the DRC reflects the inhomogeneous contribution to the diffracted signal in depth, resulting from the interference of layers with varying lattice parameters [48,49]. The profile of deformation distribution in depth changes continuously due to the propagation of the screening bound. The screening field directed along [001] induces strong piezoelectric deformation in that direction due to the coefficient d_{33} and much weaker along the orthogonal axes [50]. Thus, the strain wave propagates along the [001] direction as well. The above-described mechanism is schematically illustrated in Fig. 4. This model is supported by the results obtained for nominally pure LN [Figs. 2(c) and 3(b)]. Due to the presence of impurities and defects, this crystal also exhibits a time-delayed response to the laser pulse impact within the same time window. However, the magnitude of the observed effect in the undoped sample is noticeably less pronounced. With lower impurity concentrations in the crystal, the efficiency of compensating fields decreases, resulting in incomplete screening by photoinduced carriers. Beyond the main line of the narrative, the discovered hints on dependence of the DRC parameters on the optical polarization can be noted. The rotation of the optical polarization by $\pi/2$ reduces the magnitude of the effect by almost an order of magnitude, supporting the BPE nature of the described effect [44].

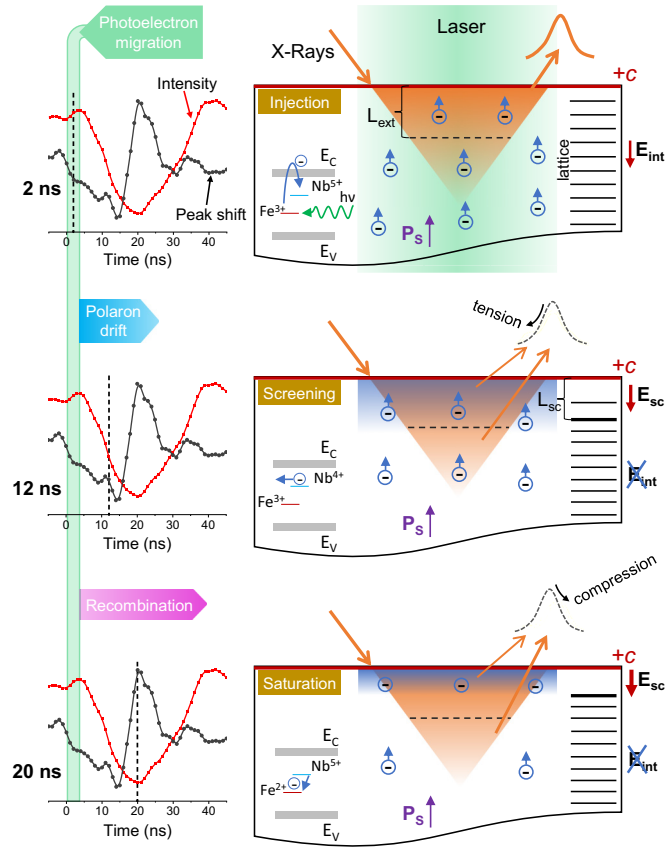

FIG. 4. Schematic representation of the rocking-curve-parameter evolution during the photoelectrons migration and the following screening electric field formation for different delays after laser illumination: (a) 2 ns, (b) 12 ns, and (c) 20 ns. E_{int} is the built-in electric field directed antiparallel to the spontaneous polarization P_S; E_{sc} is screening electric field with characteristic screening depth of L_{sc}. The resulting rocking curve forms by the depth-dependent diffraction signal which corresponds to both tensile and compression parts of the crystal lattice; L_{ext} is the extinction length of x rays

Conclusions. Using time-resolved x-ray diffractometry, we revealed an unusual time-delayed effect representing the dynamics of the formation of BPE-induced screening electric field and the resulting lattice deformations in LN : Fe crystals and nominally pure LN under the impact of a nanosecond laser pulse. The obtained dynamics of the DRCs indicates that the process of the near-surface charge layer formation and decay occurs within ~35 ns after the laser impact. The subnanosecond time resolution achieved in the experiments made it possible to study the dynamics of laser-induced processes in LN. The use of low-frequency laser pulses with comparative low fluence of ~1 J/cm^2 significantly facilitates the interpretation of the observed phenomena in the dynamics of the piezophotovoltaic effect. In general, the presented results show possibilities for obtaining information about the mechanisms of directed migration of photoelectrons, including the dynamics of the formation of charged layers and deformations in crystals.

Acknowledgments. This work was performed with the support of the Russian Science Foundation

(Grant No. 23-73-00039) using the equipment of the KISI-Kurchatov facility of NRC "Kurchatov institute" and Program of Development of Moscow University and National Project "Science and Universities".

[1] Y. Yilmaz and P. Mazumder, Nonvolatile nanopipelining logic using multiferroic single-domain nanomagnets, IEEE Trans. Very Large Scale Integr. (VLSI) Syst. **21**, 1181 (2013).

[2] K. Roy, Ultralow energy analog straintronics using multiferroic composites, IEEE Trans. Nanotechnol. **16**, 333 (2017).

[3] H. Yan, Z. Feng, S. Shang, X. Wang, Z. Hu, J. Wang, Z. Zhu, H. Wang, Z. Chen, H. Hua *et al.*, A piezoelectric, strain-controlled antiferromagnetic memory insensitive to magnetic fields, Nat. Nanotechnol. **14**, 131 (2019).

[4] N. Lei, T. Devolder, G. Agnus, P. Aubert, L. Daniel, J.-V. Kim, W. Zhao, T. Trypiniotis, R. P. Cowburn, C. Chappert *et al.*, Strain-controlled magnetic domain wall propagation in hybrid piezoelectric/ferromagnetic structures, Nat. Commun. **4**, 1378 (2013).

[5] D. Hunter, W. Osborn, K. Wang, N. Kazantseva, J. Hattrick-Simpers, R. Suchoski, R. Takahashi, M. L. Young, A. Mehta, L. A. Bendersky *et al.*, Giant magnetostriction in annealed $Co_{1-x}Fe_x$ thin-films, Nat. Commun. **2**, 518 (2011).

[6] M. Lejman, G. Vaudel, I. C. Infante, P. Gemeiner, V. E. Gusev, B. Dkhil, and P. Ruello, Giant ultrafast photo-induced shear strain in ferroelectric $BiFeO_3$, Nat. Commun. **5**, 4301 (2014).

[7] B. I. Sturman and V. M. Fridkin, *The Photovoltaic and Photorefractive Effects in Noncentrosymmetric Materials* (Gordon and Breach, New York, 1992).

[8] F. S. Pilyak, A. G. Kulikov, V. M. Fridkin, Yu. V. Pisarevsky, N. V. Marchenkov, A. E. Blagov, and M. V. Kovalchuk, Bulk piezo-photovoltaic effect in $LiNbO_3$, Phys. B: Condens. Matter **604**, 412706 (2021).

[9] H. G. Festl, P. Hertel, E. Krätzig, and R. Von Baltz, Investigations of the photovoltaic tensor in doped $LiNbO_3$, Phys. Status Solidi B **113**, 157 (1982).

[10] S. M. Young, F. Zheng, and A. M. Rappe, First-principles calculation of the bulk photovoltaic effect in bismuth ferrite, Phys. Rev. Lett. **109**, 236601 (2012).

[11] G. Dalba, Y. Soldo, F. Rocca, V. M. Fridkin, and Ph. Sainctavit, Giant bulk photovoltaic effect under linearly polarized x-ray synchrotron radiation, Phys. Rev. Lett. **74**, 988 (1995).

[12] B. Sturman, Dynamic holography effects in ferroelectrics induced by spatially oscillating photovoltaic currents, J. Opt. Soc. Am. B **8**, 1333 (1991).

[13] G. Vaudel, T. Pezeril, A. Lomonosov, M. Lejman, P. Ruello, V. Gusev, Laser generation of hypersound by a terahertz photo-Dember electric field in a piezoelectric GaAs semiconductor, Phys. Rev. B **90**, 014302 (2014).

[14] K. Buse, A. Adibi and D. Psaltis, Non-volatile holographic storage in doubly doped lithium niobate crystals, Nature (London) **393**, 665 (1998).

[15] V. M. Fridkin and B. N. Popov, Anomalous photovoltaic effect in ferroelectrics, Sov. Phys. Usp. **21**, 981 (1978).

[16] A. M. Glass, D. Von Der Linde, and T. J. Negran, High-voltage bulk photovoltaic effect and the photorefractive process in $LiNbO_3$, Appl. Phys. Lett. **25**, 233 (1974).

[17] A. Zenkevich, Yu. Matveyev, K. Maksimova, R. Gaynutdinov, A. Tolstikhina, and V. Fridkin, Giant bulk photovoltaic effect in thin ferroelectric $BaTiO_3$ films, Phys. Rev. B **90**, 161409(R) (2014).

[18] A. M. Burger, R. Agarwal, A. Aprelev, E. Schruba, A. Gutierrez-Perez, V. M. Fridkin, and J. E. Spanier, Direct observation of shift and ballistic photovoltaic currents, Sci. Adv. **5**, eaau5588 (2019).

[19] E. E. McBride, A. Krygier, A. Ehnes, E. Galtier, M. Harmand, Z. Konôpková, H. J. Lee, H.-P. Liermann, B. Nagler, A. Pelka *et al.*, Phase transition lowering in dynamically compressed silicon, Nat. Phys. **15**, 89 (2019).

[20] S. B. Brown, A. E. Gleason, E. Galtier, A. Higginbotham, B. Arnold, A. Fry, E. Granados, A. Hashim, C. G. Schroer, A. Schropp *et al.*, Direct imaging of ultrafast lattice dynamics, Sci. Adv. **5**, eaau8044 (2019).

[21] N. Huang, H. Deng, B. Liu, D. Wang, and Z. Zhao, Features and futures of x-ray free-electron lasers, The Innovation **2**, 100097 (2021).

[22] M. F. Kling and M. J. J. Vrakking, Attosecond electron dynamics, Annu. Rev. Phys. Chem. **59**, 463 (2008).

[23] A. Garmatina, E. Mareev, N. Minaev, N. Asharchuk, T. Semenov, M. Mozhaeva, A. Korshunov, Y. Krivonosov, I. Dyachkova, A. Buzmakov *et al.*, Vacuum-free femtosecond fiber laser microplasma x-ray source for radiography, Opt. Express **31**, 44259 (2023).

[24] M. M. Murnane, H. C. Kapteyn, M. D. Rosen, and R. W. Falcone, Ultrafast x-ray pulses from laser-produced plasmas, Science **251**, 531 (1991).

[25] M. Holtz, C. Hauf, A.-A. Hernández Salvador, R. Costard, M. Woerner, and T. Elsaesser, Shift-current-induced strain waves in $LiNbO_3$ mapped by femtosecond x-ray diffraction, Phys. Rev. B **94**, 104302 (2016).

[26] F. V. Potemkin, E. I. Mareev, A. A. Garmatina, M. M. Nazarov, E. A. Fomin, A. I. Stirin, V. N. Korchuganov, V. V. Kvardakov, V. M. Gordienko, V. Ya. Panchenko *et al.*, Hybrid x-ray laser-plasma/laser-synchrotron facility for pump-probe studies of the extreme state of matter at NRC "Kurchatov Institute", Rev. Sci. Instrum. **92**, 053101 (2021).

[27] N. Marchenkov, E. Mareev, A. Kulikov, F. Pilyak, E. Ibragimov, Y. Pisarevskii, and F. Potemkin, Hybrid approach for multiscale and multimodal time-resolved diagnosis of ultrafast processes in materials via tailored synchronization of laser and x-ray sources at MHz repetition rates, Optics **5**, 1 (2024).

[28] S. Gorfman, Sub-microsecond x-ray crystallography: Techniques, challenges, and applications for materials science, Cryst. Rev. **20**, 210 (2014).

[29] N. V. Marchenkov, A. G. Kulikov, A. A. Petrenko, Yu. V. Pisarevsky, and A. E. Blagov, Laboratory time-resolved x-ray diffractometry for investigation of reversible structural changes induced in single crystals by external electric field, Rev. Sci. Instrum. **89**, 095105 (2018).

[30] See Supplemental Material at http://link.aps.org/supplemental/10.1103/PhysRevB.110.L100302 for full description of the experimental setup and methodology.

[31] D. Maxein, J. Bückers, D. Haertle, and K. Buse, Photorefraction in $LiNbO_3$:Fe crystals with femtosecond pulses at 532 nm, Appl. Phys. B **95**, 399 (2009).

[32] T. Endo, S. Tani, H. Sakurai, and Y. Kobayashi, Probing thermal dissipation dimensionality to laser ablation in the pulse duration range from 300 fs to 1 μs, Opt. Express **31**, 36027 (2023).

[33] V. E. Gusev and A. A. Karabutov, *Laser Optoacoustics*, NASA STI/Recon Technical Report A, Vol. 93 (AIP, New York, 1991), p. 16842.

[34] R. Gu, V. Juvé, C. Laulhé, H. Bouyanfif, G. Vaudel, A. Poirier, B. Dkhil, P. Hollander, C. Paillard, M. C. Weber *et al.*, Temporal and spatial tracking of ultrafast light-induced strain and polarization modulation in a ferroelectric thin film, Sci. Adv. **9**, eadi1160 (2023).

[35] P. Babilotte, P. Ruello, G. Vaudel, T. Pezeril, D. Mounier, J.-M. Breteau, and V. Gusev, Picosecond acoustics in *p*-doped piezoelectric semiconductors, Appl. Phys. Lett. **97**, 174103 (2010).

[36] D. Daranciang, M. J. Highland, H. Wen, S. M. Young, N. C. Brandt, H. Y. Hwang, M. Vattilana, M. Nicoul, F. Quirin, J. Goodfellow *et al.*, Ultrafast photovoltaic response in ferroelectric nanolayers, Phys. Rev. Lett. **108**, 087601 (2012).

[37] R. T. Smith and F. S. Welsh, Temperature dependence of the elastic, piezoelectric, and dielectric constants of lithium tantalate and lithium niobate, J. Appl. Phys. **42**, 2219 (1971).

[38] L.-H. Peng, Y.-C. Fang, and Y.-C. Lin, Polarization switching of lithium niobate with giant internal field, Appl. Phys. Lett. **74**, 2070 (1999).

[39] V. Gopalan and M. C. Gupta, Origin and characteristics of internal fields in $LiNbO_3$ crystals, Ferroelectrics **198**, 49 (1997).

[40] I. Camlibel, Spontaneous polarization measurements in several ferroelectric oxides using a pulsed-field method, J. Appl. Phys. **40**, 1690 (1969).

[41] B. Sturman, M. Carrascosa, and F. Agullo-Lopez, Light-induced charge transport in $LiNbO_3$ crystals, Phys. Rev. B **78**, 245114 (2008).

[42] Z. Lu, K. Zhao, and X. Li, Photovoltaic effect in ferroelectric $LiNbO_3$ single crystal, in *Ferroelectrics—Physical Effects*, edited by M. Lallart (InTech, London, 2011).

[43] M. Nakamura, S. Horiuchi, F. Kagawa, N. Ogawa, T. Kurumaji, Y. Tokura, and M. Kawasaki, Shift current photovoltaic effect in a ferroelectric charge-transfer complex, Nat. Commun. **8**, 281 (2017).

[44] V. M. Fridkin, Bulk photovoltaic effect in noncentrosymmetric crystals, Cryst. Rep. **46**, 654 (2001).

[45] O. F. Schirmer, M. Imlau, and C. Merschjann, Bulk photovoltaic effect of $LiNbO_3$:Fe and its small-polaron-based microscopic interpretation, Phys. Rev. B **83**, 165106 (2011).

[46] Y. Qiu, K. B. Ucer and R. T. Williams, Formation time of a small electron polaron in $LiNbO_3$: Measurements and interpretation, Phys. Status Solidi C **2**, 232 (2005).

[47] S. Sasamoto, J. Hirohashi, and S. Ashihara, Polaron dynamics in lithium niobate upon femtosecond pulse irradiation: Influence of magnesium doping and stoichiometry control, J. Appl. Phys. **105**, 083102 (2009).

[48] V. G. Kohn and A. Kazimirov, Simulations of Bragg diffraction of a focused x-ray beam by a single crystal with an epitaxial layer, Phys. Rev. B **75**, 224119 (2007).

[49] A. G. Kulikov, A. E. Blagov, A. S. Ilin, N. V. Marchenkov, Yu. V. Pisarevskii, and M. V. Kovalchuk, Anisotropy and kinetics of the migration-induced layer formation in TeO_2, J. Appl. Phys. **127**, 065106 (2020).

[50] R. E. Newnham, *Properties of Materials: Anisotropy, Symmetry, Structure* (Oxford University Press, Oxford, 2005).